



## Standalone Interferometry-Based Calibration of Convex Lens-Induced Confinement Microscopy with Nanoscale Accuracy

|                               |  |
|-------------------------------|--|
| Journal:                      | <i>Analyst</i>   |
| Manuscript ID                 | AN-ART-11-2018-002300.R1   |
| Article Type:                 | Paper  |
| Date Submitted by the Author: | 12-Feb-2019  |
| Complete List of Authors:     | Morrin, Gregory; University of Colorado Boulder, Chemical and Biological Engineering<br>Kienle, Daniel; University of Colorado Boulder, Department of Chemical and Biological Engineering<br>Schwartz, Daniel; University of Colorado, Department of Chemical and Biological Engineering |
|                               |  |

1  
2  
3 **Standalone Interferometry-Based Calibration of Convex Lens-Induced**  
4  
5  
6 **Confinement Microscopy with Nanoscale Accuracy**†  
7

8  
9 Gregory T. Morrin<sup>a</sup>, Daniel F. Kienle<sup>a</sup>, and Daniel K. Schwartz<sup>\*a</sup>  
10  
11

12  
13  
14  
15 ***ABSTRACT***  
16

17 Strongly confined environments (confined dimensions between 1-100 nm) represent unique  
18 challenges and opportunities for understanding and manipulating molecular behavior due to the  
19 significant effects of electric double layers, high surface-area to volume ratios, and other  
20 phenomena at the nanoscale. Convex Lens-induced Confinement (CLiC) can be used to analyze  
21 the dynamics of individual molecules or particles confined in a planar slit geometry with  
22 continuously varying gap thickness. We describe an interferometry-based method for precise  
23 measurement of the slit pore geometry. Specifically, this approach permitted accurate  
24 characterization of separation distances as small as 5 nm, with 1 nm precision, without a priori  
25 knowledge or assumptions about the contact geometry, as well as a greatly simplified  
26 experimental setup that required only a lens, coverslip, and inverted microscope. The  
27 interferometry-based measurement of gap height offered a distinct advantage over conventional  
28 fluorescent dye-based methods; e.g., accurate interferometric height measurements were made at  
29 low gap heights regardless of solution conditions, while the concentration of fluorescent dye was  
30 significantly impacted by solution conditions such as ionic strength or pH. The accuracy of the  
31 interferometric measurements was demonstrated by comparing the experimentally measured  
32  
33  
34  
35  
36  
37  
38  
39  
40  
41  
42  
43  
44  
45  
46  
47  
48  
49  
50  
51

52  
53 <sup>a</sup> Department of Chemical and Biological Engineering,  
54 University of Colorado Boulder, Boulder, CO, 80309  
55 Email: daniel.schwartz@colorado.edu

56 † Electronic supplementary information (ESI) available.  
57  
58  
59  
60

1  
2  
3 concentration of a charged fluorescent dye as a function of gap thickness with dye concentration  
4  
5 profiles calculated using Debye-Hückel theory. Accurate characterization of nanoscale gap  
6  
7 thickness will enable researchers to study a variety of practical and biologically relevant systems  
8  
9  
10 within the CLiC geometry.  
11  
12  
13  
14  
15  
16  
17  
18  
19  
20  
21  
22  
23  
24  
25  
26  
27  
28  
29  
30  
31  
32  
33  
34  
35  
36  
37  
38  
39  
40  
41  
42  
43  
44  
45  
46  
47  
48  
49  
50  
51  
52  
53  
54  
55  
56  
57  
58  
59  
60

## ***INTRODUCTION***

Confined nanoscale geometries represent unique environments for studying the dynamics of particles and macromolecules due to the significant effects of electric double layers between charged surfaces, large surface area-to-volume ratios, and characteristic dimensions that are similar in size to a variety of biomolecules and nanoparticles<sup>1-6</sup>. These properties have been leveraged for a number of practical applications; recent advances in bioseparations<sup>7-9</sup>, biosensing<sup>10-13</sup>, single molecule analysis<sup>14-17</sup>, and the understanding of solvent behavior within interface-rich environments<sup>18</sup> have been made possible by studying and manipulating molecular behavior in nano-confinement. Producing and characterizing these highly confined environments in an accessible way remains a key challenge for researchers<sup>19-23</sup>.

Convex Lens-induced Confinement (CLiC) has shown significant promise in addressing this challenge. In their seminal publication on the method, Cohen and coworkers<sup>24</sup> showed that a wide range of gap heights (i.e., confined liquid film thickness) from several  $\mu\text{m}$  down to the nanoscale could be created by placing a convex lens in contact with a glass coverslip, which was used to study the behavior of molecules in solution. The confinement of individual molecules enabled longer tracking times and the observation of single molecules at higher analyte concentrations (due to the reduced background fluorescence) when compared to other methods such as total internal reflection fluorescence and confocal microscopy, as well as provided an effective nanoslit geometry in which the behavior of particles at various gap heights could be studied<sup>24</sup>. These methods were extended by the Leslie lab, which demonstrated various applications of the CLiC geometry through the determination of free energies of confinement<sup>25</sup>, electric-field assisted free energies within confinement<sup>26</sup>, and DNA hybridization events (determined using Förster Resonance Energy Transfer or FRET)<sup>27</sup>.

1  
2  
3 Previous CLiC experiments focused mainly on dynamics within environments with  
4 characteristic confinement dimensions in the range of several hundred nm to several  $\mu\text{m}$ , where  
5 the gap thickness was readily characterized with little ambiguity. In experiments that explored  
6 smaller gap dimensions, measurements of gap size employed implicit assumptions about solution  
7 conditions, which might not be appropriate at low ionic strengths, and a simplified view of the  
8 contact mechanics between the lens and coverslip, which could significantly affect the gap  
9 profile at small separation distances. While gap heights on the order of a hundred nanometers or  
10 higher are relevant to many industrial and biological applications, there are many situations  
11 where smaller gap heights are critically important. Many separations techniques, including  
12 protein separation using ultrafiltration<sup>28,29</sup>, as well as recent analytical methods such as  
13 electrochemical correlation spectroscopy<sup>30</sup> occur within environments that have confined  
14 dimensions on the order of tens of nanometers. Within the evolving field of nanofluidics, there  
15 remain unique challenges as well as opportunities associated with strongly confined molecular  
16 transport (confined dimensions between 1-100 nm)<sup>31</sup>. For example, Renaud and co-workers  
17 found that protein diffusion within 50 nm channels was significantly impacted by the high  
18 surface area-to-volume ratio of the channel, which increased the frequency of reversible surface  
19 interactions, and was also impacted by electric double layer effects within the channel, which  
20 substantially altered the effective volume available for diffusion<sup>32</sup>. Additionally, theoretical  
21 studies where critical polyelectrolyte adsorption within confinement was simulated (using a  
22 range of parameters pertinent to applications such as nucleic acid adsorption within viral capsids)  
23 were performed at slit heights of approximately 10 nm, where the authors found non-monotonic  
24 adsorption behavior as a function of ionic strength due to the interplay of electrostatic forces  
25 (enhanced by overlapping electric double layers) and entropic penalties<sup>33</sup>. Here, we present  
26  
27  
28  
29  
30  
31  
32  
33  
34  
35  
36  
37  
38  
39  
40  
41  
42  
43  
44  
45  
46  
47  
48  
49  
50  
51  
52  
53  
54  
55  
56  
57  
58  
59  
60

1  
2  
3 methods to extend the measurement of the confined CLiC gap thickness down to these smaller  
4  
5 nanoscale dimensions in order to more accurately measure molecular and particle dynamics at  
6  
7 the sub-100 nm scale.  
8  
9

10 Here, we enhanced the capabilities of the CLiC method by accurately characterizing gap  
11 heights down to 5 nm using an interferometric method that was not influenced by variations in  
12 ionic strength and did not require the addition of other reagents, such as fluorescent dye.  
13 Moreover, this allowed us to implement a simple and experimentally accessible realization of the  
14 CLiC geometry, which did not require the use of counterweighted lens holders or additional  
15 mechanical fixtures. In order to validate the accuracy of the interferometrically measured height  
16 profile, experimental measurements of fluorescent dye concentration profiles (vs. gap height)  
17 were made at various values of ionic strength and compared to theoretical predictions based on  
18 the Poisson-Boltzmann equation.  
19  
20  
21  
22  
23  
24  
25  
26  
27  
28  
29  
30

## 31 ***EXPERIMENTAL***

### 32 **Imaging System & Lens/Coverslip Setup**

33  
34  
35  
36 Two lasers were used for the experiments: a 488 nm wavelength Ar-ion laser (Melles  
37 Griot) was used for interferometry measurements and a 561 nm wavelength laser (Coherent) was  
38 used to excite fluorescent dye. Details about the imaging system setup are described on page S-2  
39 of the Electronic Supporting Information (ESI). The experimental setup for the lens and  
40 coverslip was the same for both interferometric gap height characterization and fluorescent dye  
41 images. Specifically, approximately 35  $\mu$ L of solution was pipetted onto a clean coverslip resting  
42 on the microscope stage, and a lens was carefully placed immediately onto the liquid on the  
43  
44  
45  
46  
47  
48  
49  
50  
51  
52  
53  
54  
55  
56  
57  
58  
59  
60

1  
2  
3 coverslip, convex side down, using tweezers. A description of the cleaning process used for the  
4  
5 lens and coverslip can be found on page S-3 of the ESI.  
6  
7

### 8 **Interferometry-Based Height Profile Measurement**

9  
10  
11  
12 Interference patterns were analyzed using custom Matlab software. A full description of  
13  
14 the image analysis and height determination is provided on pages S-4 through S-7 of the ESI.  
15  
16 Briefly, the center of the contact region of the interference pattern was determined by finding the  
17  
18 centroid of the first interference ring. Radially averaged intensities were then calculated as a  
19  
20 function of distance from the center, which were used as inputs for the height calculations. The  
21  
22 heights were determined numerically using a multilayer-matrix method<sup>34</sup> which describes the  
23  
24 propagation of light through stratified media using optical transfer matrices. Specifically, the  
25  
26 theoretical transmissivity was calculated as a function of the gap height using a previously  
27  
28 described software algorithm<sup>35</sup>. The theoretical and experimentally measured (radially averaged)  
29  
30 intensities were rescaled such that a value of 0 represented the intensity in the contact patch, and  
31  
32 a value of 1 represented the intensity of the first interference peak (determined for experimental  
33  
34 data as the maximum of the intensity data, smoothed using a Savitzky-Golay filter). The gap  
35  
36 height was then computationally determined as the height that minimized the difference between  
37  
38 the theoretical and experimental transmissivities (for a complete description, please see the ESI).  
39  
40  
41  
42  
43  
44

### 45 **Measurement of the Height Profile Using Fluorescent Dyes**

46  
47  
48 Alexa Fluor 555 dye (Invitrogen, Cat No. 20009) was added at a concentration of 8  $\mu\text{M}$   
49  
50 to aqueous solutions of varying ionic strength that were prepared using sodium chloride (Acros  
51  
52 Organics) dissolved in ultrapure water. Images of the bulk dye solution within the CLiC  
53  
54 geometry were analyzed in Matlab. In order to calculate height profiles from dye images, dye  
55  
56  
57  
58  
59  
60

1  
2  
3 intensities were converted to height using a proportionality constant based on the intensity of the  
4 dye at the radial location of the first interference fringe, where the gap height was known  
5 accurately (see ESI **Table S-1** for proportionality constant values).  
6  
7  
8  
9

### 10 **Dye Concentration Profile Measurement**

11  
12  
13 Experimental measurements of dye concentration as a function of height were obtained  
14 from images of the dye solution within the CLiC geometry. For a detailed description of the  
15 analysis, see pages S-9 through S-11 of the ESI. Briefly, the center of the contact region in the  
16 dye image was determined by fitting the intensity values within the image to a second order two-  
17 dimensional polynomial, and radially averaged intensities were then calculated as a function of  
18 distance from the center of the contact region. Dye intensity profiles were then converted to  
19 concentration using a proportionality constant that was found by fitting the intensity profile at  
20 gap sizes with fully developed electrical double layers (defined as heights greater than six Debye  
21 lengths).  
22  
23  
24  
25  
26  
27  
28  
29  
30  
31  
32  
33  
34

## 35 ***RESULTS & DISCUSSION***

### 36 **Interferometric Height Profile Measurement**

37  
38  
39 The height profile of the lens as a function of distance from the center of the contact  
40 region is shown in **Figure 1**. We assume that the initial, relatively noisy region near the center  
41 of the contact region corresponded to the upper bound of the radius of contact between the lens  
42 and the coverslip. Since both the lens and coverslip were considered linear elastic materials  
43 (fused silica and borosilicate glass, respectively) they were expected to deform when the lens  
44 was placed on the coverslip due to the applied load. This produced a circular region of contact  
45 whose dimensions could be theoretically calculated and compared to experimental  
46  
47  
48  
49  
50  
51  
52  
53  
54  
55  
56  
57  
58  
59  
60



1  
2  
3 measurements; in our case, Hertzian assumptions were made in order to estimate the contact  
4 region since the surfaces were not molecularly smooth and had some degree of roughness<sup>36</sup>. At  
5 the Hertzian limit, the radius of the contact region could be determined using the relationship<sup>36</sup>:  
6  
7  
8  
9

$$10 \quad a = \sqrt[3]{\frac{3FR}{4E^*}} \quad (1)$$

11  
12  
13  
14 Where  $a$  represented the radius of the contact region,  $F$  represented the loading force,  $R$   
15 represented the radius of the lens, and  $E^*$  represented the reduced modulus of the glass surfaces.  
16  
17 Parameters that were used for the equation are described on page S-12 of the ESI. The  
18 theoretical contact region radius,  $a$ , was approximately 15  $\mu\text{m}$ , which was in reasonable  
19 agreement with the measured radius of the contact region. The contribution of coverslip flexure  
20 to the contact region did not appear to have a significant effect on the contact radius, as  
21 evidenced by the good agreement of the measured contact radius and theoretical Hertzian contact  
22 radius (which assumes an elastic half-space). Outside of the contact region, height  
23 measurements down to approximately 5 nm were determined to have uncertainties of  
24 approximately 1 nm, as indicated by the confidence intervals on the height profile. We noted that  
25 there was a significantly higher degree of noise within the profile at heights that corresponded to  
26 the first interference fringe (approximately 92 nm) when compared to the rest of the height  
27 profile. This was due to the fact that the variation of height with intensity followed an inverse  
28 cosine function<sup>37</sup>, which has its steepest slopes at the peak and trough of the interference fringes,  
29 such that small fluctuations in the intensity caused large errors in the height calculation.  
30  
31  
32  
33  
34  
35  
36  
37  
38  
39  
40  
41  
42  
43  
44  
45  
46  
47  
48  
49  
50  
51  
52  
53  
54  
55  
56  
57  
58  
59  
60

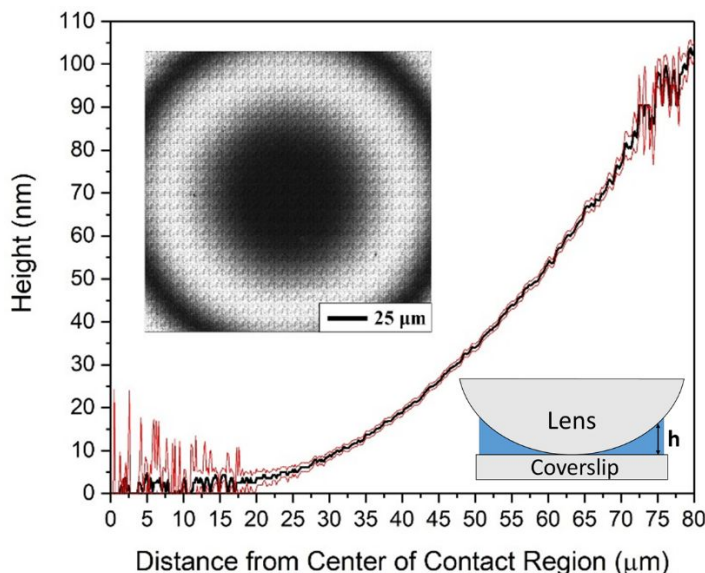


**Figure 1.** Height profile of the gap between lens and coverslip as a function of distance from the center of the contact region (black line). Red lines represent 95% confidence intervals. Inset, upper left: Multiple field-of-view interference pattern used to determine the height profile. Inset, lower right: diagram illustrating the CLiC geometry.

### Interferometric Height Comparison with Dye Height Profile Measurements

While interferometry-based measurements of the height profile were previously used for gap heights greater than or equal to the height corresponding to the first interference fringe (due to the formation of Newton's rings<sup>38</sup>), they were not employed to measure smaller CLiC gap heights. In fact, the most common approach to measure the height for these smaller gap thicknesses (i.e. smaller than the thickness associated with the first interference fringe) required the penetration of fluorescent dye into the gap, where emission intensity was measured as a function of radial position<sup>24,25,39-41</sup>. This method was most accurate in the limit where dye molecules had negligible interactions with the confining surfaces (such as electrostatic interactions) as well as minimal adsorption at these interfaces. Assuming these criteria were met, the intensity at a given pixel would be proportional to the height at that point<sup>24</sup>. However, ionic

1  
2  
3 strength could significantly affect the electrostatic interactions between dyes and the surfaces  
4  
5 confining them, particularly when the gap height was on the order of the Debye length in  
6  
7 solution <sup>42</sup>. Moreover, surface adsorption could also potentially skew such interpretations. We  
8  
9 measured the intensity of a negatively charged fluorescent dye molecule within the gap between  
10  
11 the lens and coverslip (both of which were also negatively charged) under conditions where a  
12  
13 significant degree of electrostatic dye exclusion was observed. As shown in **Figure 2A-C**, the  
14  
15 penetration of dye molecules near the lens/coverslip contact region was significantly affected by  
16  
17 electrostatic effects—as shown by the shrinking of the dark excluded region—as the electrostatic  
18  
19 repulsion between the surface and the dye molecules was increasingly screened by higher  
20  
21 concentrations of sodium counter-ions. These qualitative differences were reflected in the  
22  
23 apparent height profiles calculated from the intensity measurements (see **Figure 2D**). Clearly,  
24  
25 the apparent height profiles measured using dye intensities required significant corrections in  
26  
27 order to account for the repulsive interactions that reduced dye concentration at these small gap  
28  
29 heights.  
30  
31  
32  
33  
34  
35  
36  
37  
38  
39  
40  
41  
42  
43  
44  
45  
46  
47  
48  
49  
50  
51  
52  
53  
54  
55  
56  
57  
58  
59  
60

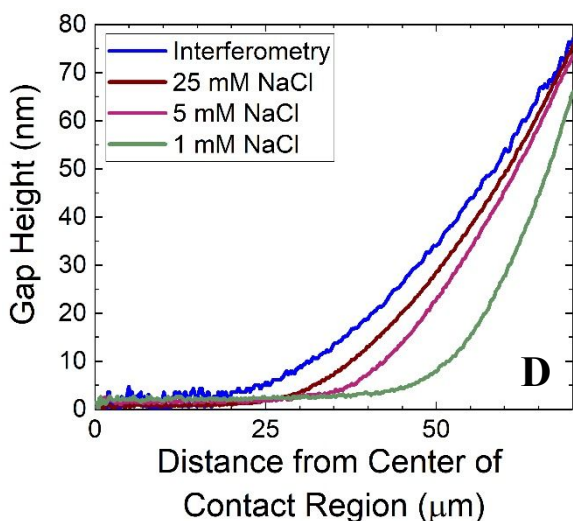
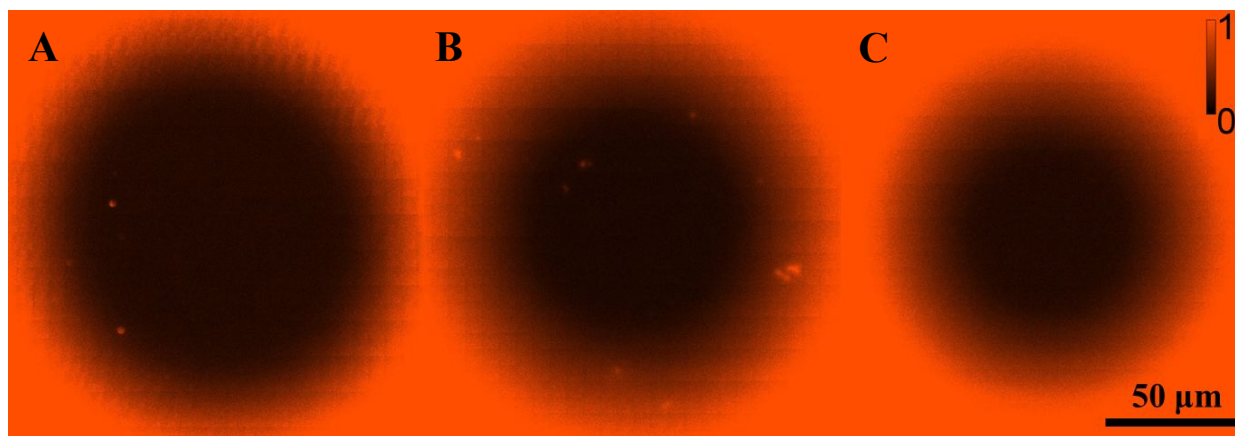


**Figure 2.** Images of fluorescent dye near the lens/cover slip contact region for (A) 1 mM, (B) 5 mM, and (C) 25 mM NaCl. A color scale bar is presented in the upper right corner that defines the normalized intensity range of the images. (D) Comparison of apparent height profiles calculated using the traditional dye-intensity method at various salt concentrations with the height profile measured using the interferometric approach.

As the salt concentration was increased the profiles systematically approached the interferometric profile, consistent with expectations as the electrostatic repulsion of dye molecules was increasingly screened, which permitted better penetration of the dye, and resulted in improved height characterization. However, this limited the utility of dye-intensity gap thickness characterization to high ionic strength conditions. Moreover, as the ionic strength was increased, it was common to observe additional intensity artifacts due to increased surface adsorption.

### Experimental Measurement Comparison with Theoretical Predictions

In order to validate the accuracy of the interferometry-based height measurements, the concentration of dye as a function of height was experimentally determined and compared to theoretical predictions based on the Poisson-Boltzmann equation. The theoretical model was based on the work done by Renaud and co-workers studying dye diffusion in glass nanochannels<sup>6,42</sup>, where a Boltzmann distribution was used to describe the equilibrium concentration of various ions in solution as a function of electric potential (assumed to vary only in the direction normal to the glass surfaces):

$$C_i(z) = C_{B,i} \exp\left[-\frac{q * \psi(z)}{k_B T}\right] \quad (2)$$

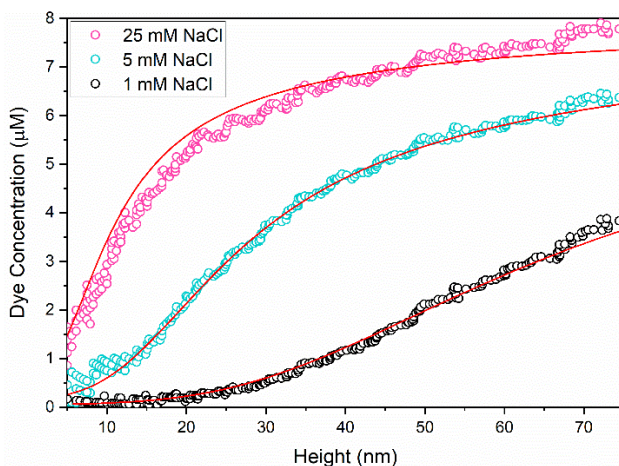
Where  $C_i$  represented the concentration of a particular ion at a distance  $z$  from the surface,  $C_{B,i}$  represented the bulk concentration of the ion,  $q$  represented the charge of the ion,  $\psi(z)$  represented the electric potential at a distance  $z$  from the surface,  $k_B$  represented the Boltzmann constant, and  $T$  represented the temperature. The expression for the electric potential was derived using the Debye-Hückel approximation<sup>6</sup>, a linearized form of the Poisson-Boltzmann equation appropriate under these conditions, which leads to the following analytical expression:

$$\psi(z) = \frac{\zeta \cosh\left[\left(\frac{h}{2} - z\right)/\lambda_D\right]}{\cosh\left(\frac{h}{2\lambda_D}\right)} \quad (3)$$

where  $\zeta$  represented the zeta potential of the surface,  $h$  represented the gap height,  $z$  represented the distance from the surface, and  $\lambda_D$  represented the Debye length of the solution. The parameters used to calculate the electric potential, such as the zeta potential and Debye length, are described on pages S-13 and S-14 of the ESI. The average predicted concentration of dye for

1  
2  
3 a given gap height was calculated by integrating the theoretical concentration over the entire  
4 height of the slit, and dividing by the slit height.  
5  
6

7  
8 In order to compare the theoretical calculations directly to experimental data,  
9  
10 measurements of the intensity as a function of height were converted to concentration (see pages  
11 S-9 through S-11 of the ESI). Comparisons between theoretical calculations and experimental  
12 results are shown in **Figure 3**. Overall, good agreement was found between the experimental  
13 data and theoretical predictions, confirming that the height measurements from the  
14 interferometry-based approach were accurate. Importantly, the concentration of dye at all levels  
15 of ionic strength tested were significantly different from the bulk concentration over a large  
16 range of heights at the nanoscale. Within this region, the penetration of dye was strongly  
17 impacted by electrostatic forces, illustrating both the unique phenomena that occur at this length  
18 scale as well as the need for a method that could measure gap heights without being affected by  
19 solution conditions such as ionic strength.  
20  
21  
22  
23  
24  
25  
26  
27  
28  
29  
30  
31  
32  
33



34  
35  
36  
37  
38  
39  
40  
41  
42  
43  
44  
45  
46  
47  
48  
49  
50 **Figure 3.** Dye concentration plotted as a function of gap height for various salt concentrations.  
51 Experimental measurements are represented by open circles ( $\circ$ ) and theoretical predictions are  
52 represented by red lines. Confidence intervals were smaller than the symbols representing the  
53 experimental data. Data was cut off at 5 nm due to greater uncertainty at low intensities.  
54  
55  
56  
57  
58  
59  
60

## CLiC Method Comparison and Current System Limitations

Previous measurements of very small gap heights in CLiC systems did not explicitly account for contact mechanics between the glass coverslip and lens, which lead to a contact area (“patch”) as opposed to a single point of contact, as frequently assumed. Assumptions related to the contact mechanics between the lens and coverslip can have a significant effect on the calculated height profile below the first interference fringe. In previous studies, dye intensity measurements used to determine the height profile included the entire region around the contact point and assumed non-zero height, rather than accounting for a contact region using a constant average intensity and zero gap height. As described above, we found that deformations due to contact mechanics had a particularly large influence in the small gap thickness regime. Even if counterweights were used to reduce the load due to the effective weight of the lens, a significant contact region is expected to form due to the residual weight, in addition to other attractive forces including capillary interactions and van der Waals forces. For example, if a counterweight was used to offset approximately 90% of the weight of the lens, as in previous work<sup>24</sup>, this would still result in a contact region with a radius of at least 7  $\mu\text{m}$ , assuming common literature values for the elastic moduli and Poisson ratios of the coverslip and lens, but ignoring additional loading due to other attractive interactions. While the effect of the contact region becomes unimportant at large radial distances, where the gap height is large, it significantly influences the accuracy of the profile in the small gap thickness regime. This may explain apparent discrepancies previously reported between the actual molecular dimensions and those inferred from dye intensity measurements, where molecular diameters inferred from exclusion at small gap height consistently overestimated their known sizes<sup>24</sup>. Notably, some recent CLiC implementations attempted to account for contact area phenomena<sup>40</sup>. Experiments

1  
2  
3 that focus on phenomena involving nanoscale gaps will benefit greatly from an accurate and  
4 independent measurement of gap thickness, that does not require ad hoc assumptions about dye  
5 penetration.  
6  
7  
8  
9

10 The methods reported here provided significantly improved accuracy of CLiC height  
11 profiles, particularly in the nanoscale regime. CLiC has been effectively leveraged for single  
12 molecule studies that investigated the effects of confinement on relatively large molecules at  
13 scales ranging between about a hundred nanometers to several microns. By improving height  
14 profile measurements below the first interference fringe, confined dimensions relevant to smaller  
15 molecules can now also be performed with better precision using CLiC. Moreover, this  
16 approach enabled a greatly simplified experimental setup, that did not require complex or custom  
17 mechanical components, such as frictionless counterweights. Here, we demonstrated that  
18 experiments could readily probe the behavior of molecules with nanoscale gaps using only a  
19 lens, coverslip, and a conventional inverted microscope. By eliminating the need for free dye in  
20 solution for height estimation, potentially unwanted interactions between the fluorescent probe  
21 and the analyte of interest were avoided and the range of wavelengths available for probe  
22 excitation was expanded (a useful feature for experiments where multiple dyes may be required,  
23 such as FRET). In future studies, the interferometric approach will allow a broader range of  
24 systems to be studied with *in situ* measurements of the height profile. Additionally, by using the  
25 multilayer-matrix-method, extension to confining surfaces modified with additional  
26 independently characterized films will be possible.  
27  
28  
29  
30  
31  
32  
33  
34  
35  
36  
37  
38  
39  
40  
41  
42  
43  
44  
45  
46  
47  
48  
49

50 We also note some limitations to our approach; if flow is required or solution exchange  
51 is needed, the current experimental setup may not be sufficient, and previous CLiC  
52 implementations should be considered<sup>27,39,40,43</sup>. It is worth noting that hybrid approaches can  
53  
54  
55  
56  
57  
58  
59  
60



1  
2  
3 also be performed, where an interferometry-based approach for height measurements near the  
4 contact region can be combined with a complex, high-throughput CLiC system. For CLiC  
5 experiments where patterned surfaces may be necessary<sup>41</sup>, an interferometric approach may be  
6 difficult to implement. However, there have been a number of experiments where the CLiC  
7 geometry alone provided a suitable environment for studying the dynamics of large molecules as  
8 a function of confinement<sup>24,25,44</sup>. An extension of these types of experiments to smaller gap  
9 thickness will enable the study of molecular behavior at varying degrees of confinement that are  
10 relevant to a wide range of applications, including protein separation methods<sup>28,29</sup>,  
11 polyelectrolyte adsorption at biointerfaces<sup>45</sup>, and single-molecule sensors<sup>46</sup>.  
12  
13  
14  
15  
16  
17  
18  
19  
20  
21  
22  
23  
24  
25  
26

## 27 ***CONCLUSIONS***

28  
29  
30 An accurate method for measuring confined molecular dynamics at the nanoscale was  
31 developed based on confinement between a convex lens and a planar fused silica wafer. The  
32 accuracy of the method was validated through the agreement of experimental results with  
33 predictions from the linearized Poisson-Boltzmann equation, where negatively charged dye  
34 molecules were increasingly excluded from negatively charged gaps as the ionic strength was  
35 decreased. Using interferometry, rather than free fluorescent dyes in solution, gap heights as  
36 small as 5 nm were consistently measured with nm precision, regardless of the strength of  
37 interactions (e.g. electrostatic forces, surface affinity) within the confined environment,  
38 extending the range of heights that can be used to study single-molecule behavior in  
39 confinement. Another key advantage of the system was its experimental simplicity. The method  
40 described here will provide an easily accessible nanoscale system for researchers studying  
41 confined molecular dynamics.  
42  
43  
44  
45  
46  
47  
48  
49  
50  
51  
52  
53  
54  
55  
56  
57  
58  
59  
60

### ***CONFLICTS OF INTEREST***

There are no conflicts to declare.

### ***ACKNOWLEDGEMENTS***

The authors would like to thank Raphael Sarfati for useful discussions pertaining to the analyses.

G.T.M. and D.K.S. were supported by the U.S. Department of Energy, Office of Science, Basic Energy Sciences (award #DE-SC0001854) for data acquisition, statistical analysis, interpretation of the results, and manuscript preparation. Additional support for G.T.M.'s graduate training was provided by the NIH/CU Molecular Biophysics Graduate Traineeship T32 GM065103.

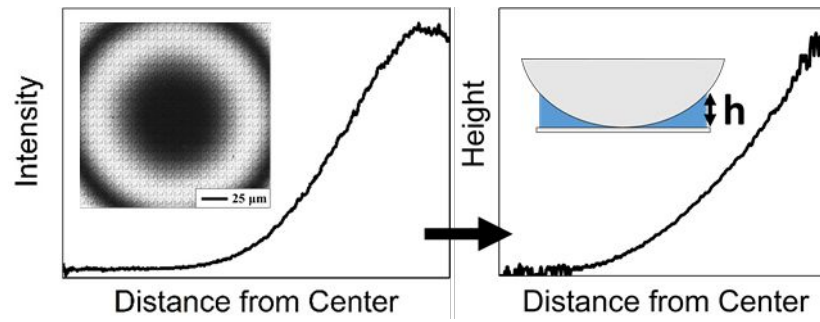
Support for D.F.K. was provided by the U.S. Defense Threat Reduction Agency (award #HDTRA1-16-1-0045) for development of data analysis methods. The imaging work was performed at the BioFrontiers Institute Advanced Light Microscopy Core. TIRF microscopy was performed on a Nikon A1R microscope supported by NIST-CU Cooperative Agreement (award #70NANB15H226). ***REFERENCES***

- 1 A. Piruska, M. Gong, J. V Sweedler and P. W. Bohn, *Chem. Soc. Rev.*, 2009, **39**, 1060–1072.
- 2 M. L. Kovarik and S. C. Jacobson, *Anal. Chem.*, 2009, **81**, 7133–7140.
- 3 P. Abgrall and N. T. Nguyen, *Anal. Chem.*, 2008, **80**, 2326–2341.
- 4 M. Napoli, J. C. T. Eijkel and S. Pennathur, *Lab Chip*, 2010, **10**, 957–985.
- 5 L. Bocquet and P. Tabeling, *Lab Chip*, , DOI:10.1039/c4lc00325j.
- 6 R. B. Schoch, J. Han and P. Renaud, *Rev. Mod. Phys.*, 2008, **80**, 839–883.
- 7 E. A. Strychalski, H. W. Lau and L. A. Archer, *J. Appl. Phys.*, 2009, **106**, 024915.
- 8 M. Bassu, P. Holik, S. Schmitz, S. Steltenkamp and T. P. Burg, *Lab Chip*, 2016, **16**, 4546–4553.
- 9 S. Pennathur and J. G. Santiago, *Anal. Chem.*, 2005, **77**, 6782–6789.
- 10 Z. D. Harms, K. B. Mogensen, P. S. Nunes, K. Zhou, B. W. Hildenbrand, I. Mitra, Z. Tan,

- 1  
2  
3 A. Zlotnick, J. Org, P. Kutter and S. C. Jacobson, *Anal. Chem*, 2011, **83**, 9573–9578.  
4  
5 11 J. Wang, J. Hou, H. Zhang, Y. Tian and L. Jiang, *ACS Appl. Mater. Interfaces*, 2018, **10**,  
6 2033–2039.  
7  
8 12 Z. Sun, T. Liao, Y. Zhang, J. Shu, H. Zhang and G.-J. Zhang, *Biosens. Bioelectron.*, 2016,  
9 **86**, 194–201.  
10  
11 13 C. Chen, Y. Li, S. Kerman, P. Neutens, K. Willems, S. Cornelissen, L. Lagae, T.  
12 Stakenborg and P. Van Dorpe, *Nat. Commun.*, 2018, **9**, 1733.  
13  
14 14 L. D. Menard and J. M. Ramsey, *Anal Chem*, 2013, **85**, 1146–1153.  
15  
16 15 W. Reisner, J. P. Beech, N. B. Larsen, H. Flyvbjerg, A. Kristensen and J. O. Tegenfeldt,  
17 *Phys. Rev. Lett.*, 2007, **99**, 058302.  
18  
19 16 G. F. Schneider, S. W. Kowalczyk, V. E. Calado, G. Pandraud, H. W. Zandbergen, L. M.  
20 K. Vandersypen and C. Dekker, *Nano Lett.*, 2010, **10**, 3163–3167.  
21  
22 17 X. Liang and S. Y. Chou, *Nano Lett.*, 2008, **8**, 1472–1476.  
23  
24 18 T. Tsukahara, W. Mizutani, K. Mawatari and T. Kitamori, *J. Phys. Chem. B*, 2009, **113**,  
25 10808–10816.  
26  
27 19 C. Duan, W. Wang and Q. Xie, *Biomicrofluidics*, 2013, **7**, 026501.  
28  
29 20 D. Mijatovic, J. C. T. Eijkel and A. Van Den Berg, *Lab Chip*, 2005, **5**, 492–500.  
30  
31 21 D. G. Haywood, A. Saha-Shah, L. A. Baker and S. C. Jacobson, *Anal. Chem.*, 2015, **87**,  
32 172–187.  
33  
34 22 Y. Xu, *Adv. Mater.*, 2018, **30**, 1–17.  
35  
36 23 D. Xia, J. Yan and S. Hou, *Small*, 2012, **8**, 2787–2801.  
37  
38 24 S. R. Leslie, A. P. Fields and A. E. Cohen, *Anal. Chem.*, 2010, **82**, 6224–6229.  
39  
40 25 J. S. Leith, A. Kamanzi, D. Sean, D. Berard, A. C. Guthrie, C. M. J. Mcfaul, G. W. Slater,  
41 H. W. De Haan and S. R. Leslie, *Macromolecules*, 2016, **49**, 9266–9271.  
42  
43 26 M. J. Ahamed, S. Mahshid, D. J. Berard, F. O. Michaud, R. Sladek, W. W. Reisner and S.  
44 R. Leslie, *Macromolecules*, 2016, **49**, 2853–2859.  
45  
46 27 A. Arsenault, J. S. Leith, G. Henkin, C. M. J. Mcfaul, M. Tarling, R. Talbot, D. Berard, F.  
47 Michaud, S. Scott and S. R. Leslie, *Rev. Sci. Instrum.*, 2015, **86**, 033701.  
48  
49 28 C. Zhou, T. Segal-Peretz, M. E. Oruc, H. S. Suh, G. Wu and P. F. Nealey, *Adv. Funct.*  
50 *Mater.*, 2017, **27**, 1701756.  
51  
52 29 P. Stroeve, M. Rahman, L. D. Naidu, G. Chu, M. Mahmoudi, P. Ramirez and S. Mafe,  
53 *Phys. Chem. Chem. Phys.*, 2014, **16**, 21570.  
54  
55 30 D. Magde, W. W. Webb, E. Elson, M. Eigen, R. Rigler, U. Bertocci, C. Gabrielli, F. Huet,  
56 M. Keddam and P. Rousseau, *Proc. Natl. Acad. Sci. U. S. A.*, 1972, **29**, 8203–8212.  
57  
58  
59  
60

- 1  
2  
3 31 S. L. Bocquet, P. Tabeling and L. Bocquet, *Lab Chip*, 2014, **14**, 3143–3158.  
4  
5 32 N. F. Durand, C. Dellagiacomma, R. Goetschmann, A. Bertsch, I. Märki, T. Lasser and P.  
6 Renaud, *Anal. Chem.*, 2009, **81**, 5407–5412.  
7  
8 33 S. J. De Carvalho, R. Metzler and A. G. Cherstvy, *Soft Matter*, 2015, **11**, 4430–4443.  
9  
10 34 M. Born and E. Wolf, *Principles of Optics*, Pergamon, Oxford, U.K., 6th edn., 1980.  
11  
12 35 D. F. Kienle and T. L. Kuhl, *Anal. Chem.*, 2014, **86**, 11860–11867.  
13  
14 36 J. Israelachvili, *Intermolecular and Surface Forces*, Elsevier, San Diego, 3rd edn., 2011.  
15  
16 37 K. D. Moller, in *Optics: Learning by Computing with Examples Using MathCAD*,  
17 Springer, New York, 2003, pp. 77–125.  
18  
19 38 G. B. Airy, *London, Edinburgh, Dublin Philos. Mag. J. Sci.* 2.7, 1833, 20–33.  
20  
21 39 S. Mahshid, M. J. Ahamed, D. Berard, S. Amin, R. Sladek, S. R. Leslie and W. W.  
22 Reisner, *Lab Chip*, 2015, **15**, 3013.  
23  
24 40 D. Berard, C. M. J. McFaul, J. S. Leith, A. K. J. Arsenault and F. Michaud, *Rev. Sci.*  
25 *Instrum*, 2013, **84**, 103704.  
26  
27 41 D. J. Berard, F. Michaud, S. Mahshid, M. J. Ahamed, C. M. J. McFaul, J. S. Leith, P.  
28 Bérubé, R. Sladek, W. Reisner and S. R. Leslie, *PNAS*, 2014, **111**, 13295–13300.  
29  
30 42 A. Plecis, R. B. Schoch and P. Renaud, *Nano Lett.*, 2005, **5**, 1147–1155.  
31  
32 43 S. Scott, Z. Ming Xu, F. Kouzine, D. J. Berard, C. Shaheen, B. Gravel, L. Saunders, A.  
33 Hofkirchner, C. Leroux, J. Laurin, D. Levens, C. J. Benham and S. R. Leslie, *Nucleic*  
34 *Acids Res.*, 2018, **46**, 4622–4631.  
35  
36 44 C. M. J. McFaul, J. Leith, B. Jia, F. Michaud, A. Arsenault, A. Martin, D. Berard and S.  
37 Leslie, in *Proc. SPIE 8811, Physical Chemistry of Interfaces and Nanomaterials XII*,  
38 2013, p. 881102.  
39  
40 45 A. G. Cherstvy, *Biopolymers*, 2012, **97**, 311–317.  
41  
42 46 K. Ando, M. Tanabe and K. Morigaki, *Langmuir*, 2016, **32**, 7958–7964.  
43  
44  
45  
46  
47  
48  
49  
50  
51  
52  
53  
54  
55  
56  
57  
58  
59  
60

## Table of Contents Entry



Interferometry-based measurement of gap height in convex lens-induced confinement significantly improves accuracy at sub-100 nm gap thickness.